Comp. Meth. Civil Eng., Vol. 2 No. 1 (2011) 1-20

CMCE
Computational Methods in Civil Engineering

Invited Paper

A dynamic lattice model for heterogeneous materials

A.R. Khoei*, M.H. Pourmatin

Center of Excellence in Structural and Earthquake Engineering, Department of Civil Engineering, Sharif University of Technology, P.O. Box. 11365-9313, Tehran, Iran

Received 17 September 2010

Abstract

In this paper, the mechanical behavior of three-phase inhomogeneous materials is modeled using the meso-scale model with lattice beams for static and dynamic analyses. The Timoshenko beam theory is applied instead of the classical Euler-Bernoulli beam theory and the mechanical properties of lattice beam connection are derived based on the continuum medium using the non-local continuum theory. The average acceleration method is applied for dynamic modeling of crack propagation in concrete. Finally, two experimental tests, including the simple tension experiment and the Nooru-Mohamed test, are simulated using the proposed model in order to investigate the effects of dynamic crack propagation, and the results are compared with those of static analysis.

Keywords: Lattice model; Beam element; Crack pattern; Dynamic behavior.

1. Introduction

Numerical analysis of crack propagation and fracture process in inhomogeneous materials, such as concrete, has always been a challenging issue. Various methods have been used by researchers depending on the available computer capacities. Damage models have been the center of attention for more than three decades according to their computational feasibility. Although these models have given satisfactory results for material behavior, they are not pertinent alternatives for crack pattern simulations and micro crack observations. On the other hand, despite of considerable accuracy and economic computation effort, the fictitious crack model and crack band model are unable to simulate the crack ramification in concrete. In contrast, the lattice model, which was originally developed by Hrennikoff [1] in 1941, has the ability of a reliable crack path prediction with micro-crack observation and ramifications. Due to high computational demands the method did not gain a significant attention till 90s. Moreover, such a high computation expense has preserved researchers from any major work on the dynamic behavior of inhomogeneous materials through the lattice models.

*Corresponding author. Tel. +98 (21) 6600 5818; Fax: +98 (21) 6601 4828.
E-mail address: arkhoei@sharif.edu (A.R. Khoei)

Nomenclature

C	damping matrix
d_{ij}	the distance of center of aggregate *i* from aggregate *j*
D_i	the diameter of aggregates *i*
E^b	elastic module of lattice beam element
$\mathbf{f}$	vector of external forces
GA	shear rigidity
h	depth of lattice beam element
$\mathcal{J}$	the diagonal component of third DOF of mass matrix
$\mathbf{K}_{\text{beam}}$	stiffness matrix of a beam element
$\mathbf{K}_{\text{rod}}$	stiffness matrix of a rod element
$\mathbf{K}_{\text{rod+beam}}$	stiffness matrix of a lattice beam element
$\widehat{\mathbf{K}}$	the global stiffness matrix of lattice beam element
l	length of lattice beam element
$\mathcal{M}$	the diagonal component of first two DOFs of mass matrix
M	mass matrix
R	the depth-length ratio of lattice beam element
t	thickness of continuum medium
t^b	thickness of lattice beam element
T_n	the natural period of one single beam element
u_i	displacement vector
$\dot{u}_i$	velocity vector
$\ddot{u}_i$	acceleration vector
U_{cell}	the strain energy of a unit cell of lattice
$U_{\text{continuum}}$	the strain energy of continuum medium
α	correction factor
β	the dimensionless ratio of bending to shear stiffness
$\varepsilon_{\text{failure}}$	axial strain criterion
δ_t	the tensile prescribed displacement
δ_s	the shear prescribed displacement
Δt	time step
γ	a coefficient indicating the contribution of curvature in strain
γ_1, γ_2	the Newmark parameters
$\mathbf{\Gamma}$	rotation matrix
υ^b	Poisson ratio of lattice beam element
θ	the angle of lattice beam element with horizontal direction
ρ	density

From the scaling point of view, one can study fracture process in heterogeneous materials in various scales, including macro, meso, micro and nano scale. It is clear that the smaller scale modeling can be used by simpler constitutive laws [2]. In the macro-scale model, the material is considered as homogeneous and consequently, the constitutive laws are more complicated. However in meso-scale model, the concrete is considered as a three phase body, namely, the matrix phase, aggregate phase and the interface between these two phases.

Technically, there are two main approaches for crack propagation simulation of concrete in meso-scale model. The first method is based on the classical approach, in which the general relation between the stress and strain is calculated from corresponding experiments and the out coming material properties may not be the material property of concrete ingredients. In this method, the concrete is considered as a homogenous material, and the procedure needs less computational effort, however – it cannot predict fracture pattern accurately. The second approach simulates the material inhomogeneity physically, called as the physical-based approach. In this technique, aggregates are generated with various sizes and located with a normal statistical distribution. As a result, this approach is more realistic, but it has computational cost, since elements must be smaller than the finest aggregates [3].

The lattice model has been used and developed by various researchers. Hrennikoff [1] employed the bar elements with only two degrees of freedom at both ends. Herrmann et al. [4] proposed the beam elements instead of bar, or spring elements, with six degrees-of-freedom in 2D simulation, and 12 DOFs in 3D modeling. However, due to lower computational demand of spring elements, it is still a popular lattice model among researchers [5,6]. The disadvantage of implementation of spring elements is in prediction of mixed mode fractures, while the beam elements provide more realistic results for mixed mode fracture processes. A new generalized beam element was proposed by Liu et al. [7,8] which was composed of three different beam elements to reduce the computational expenses. In this method, the Timoshenko beam theory was used instead of the Euler–Bernoulli classical theory and some modifications were implemented into the constitutive laws. The linear lattice element was proposed by Lilliu and van Mier [9] and Schlangen and Garboczi [10] in micro- and meso-scale models. The nonlinear plastic lattice model was implemented by Cusatis et al. [11,12] in macro-scale modeling.

Fracture is generally a dynamic phenomenon and the static modeling of crack propagation – even for very low loading rates – is inherently an approximation. To the knowledge of authors, there are not major studies on dynamic modeling of fracture in concrete using the meso-scale model. In one of the rare studies of dynamic simulation of fracture in lattice modeling, Liu et al. [8] proposed a dynamic analysis using the central difference method, and compared their results with the quasi-static simulation. In the present paper, the dynamic modeling of inhomogeneous materials is performed using the meso-scale model with lattice beams. The Newmark technique based on the average acceleration method is applied for dynamic modeling of crack propagation. The Timoshenko beam theory is employed for lattice elements and their mechanical properties are derived using the non-local continuum concept. Two experimental tests are finally simulated to investigate the effects of dynamic crack propagation, for a simple tension experiment and the mixed mode fracture of Nooru-Mohamed test.

2. The lattice model

In lattice model, it is necessary to provide a relationship between the lattice parameters and the continuum medium. There are various approaches proposed by researchers to obtain this relationship. Cusatis et al. [11,12] applied the Delaunay triangulation to assign the proper area of each bar element. Kozicki and Tejchman [13] used the experimental coefficients to derive the axial and shear stiffness. However, the globally accepted approach is based on the nonlocal continuum technique to obtain the elasticity module and Poisson ratio of beam elements from corresponding continuum factors. In order to obtain the mechanical properties of lattice model, the equivalence of strain energy can be performed for a unit cell of lattice and its continuum counterpart as:

$$U_{\text{cell}} = U_{\text{continuum}} \tag{1}$$

Based on this method, the lattice mesh has to be uniform with a specific cell figure, since it is unfeasible to perform the evaluation of each single cell in random lattice model. The most common lattice shape for 2D simulation is triangular form, as shown in Figure 1, due to its simplicity and generality [14].

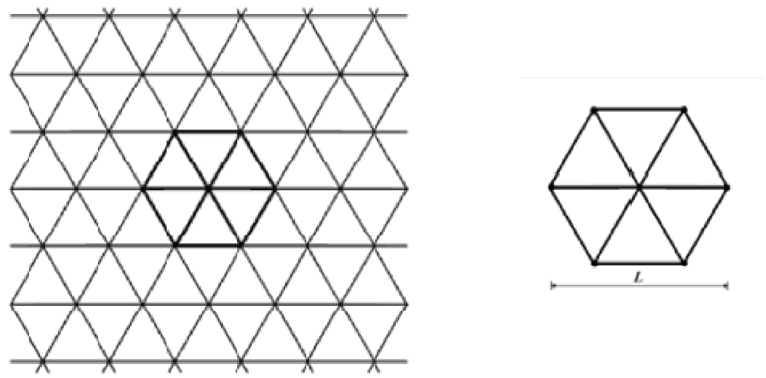

Figure 1. A regular lattice model together with a hexagonal cell.

In the nonlocal continuum concept, the relationship between the elastic module E^b and the Poisson ratio of beam elements υ^b can be written as [14]:

$$E^b = \frac{E}{2\sqrt{3}R} \frac{3 + R^2 \dfrac{1}{1+\beta}}{1 + R^2 \dfrac{1}{1+\beta}} \frac{t}{t^b} \tag{2}$$

$$\upsilon^b = \frac{1 - R^2 \dfrac{1}{1+\beta}}{1 + R^2 \dfrac{1}{1+\beta}} \tag{3}$$

in which for the Timoshenko beam, $R = h/l$ denotes the ratio of depth to length, t the thickness of continuum medium, t^b the thickness of beam element, and h the depth of beam element. In above relations, β is the dimensionless ratio of bending to shear stiffness. If $\beta = 0$, the Euler-Bernoulli beam can be derived as:

$$E^b = \frac{E}{2\sqrt{3}R} \frac{3 + R^2}{1 + R^2} \frac{t}{t^b} \tag{4}$$

$$\upsilon^b = \frac{1 - R^2}{1 + R^2} \tag{5}$$

There are various approaches to generate the aggregate distribution on lattice model. One of the most effective and random methods is based on the location of aggregates on lattice mesh in a decelerating manner. In this method, the biggest aggregate is first located randomly, then the second biggest, after that the third, the forth and *etc*. In this procedure, there is a rule, in which the current location of aggregate must not have any overlay with the previously located ones. A minimum distance between each aggregate is proposed as [11]:

$$d_{ij} \geq 1.2 \left(\frac{D_i + D_j}{2} \right) \tag{6}$$

where d_{ij} is the distance of center of aggregate i from aggregate j, and D_i and D_j are the diameters of aggregates i and j, respectively. For those elements that both ends are located in the matrix, labeled as the 'matrix', if both ends are located in aggregate, labeled as the 'aggregate', and if one end belongs to matrix and the other end to aggregate, labeled as the 'interface', as shown in Figure 2.

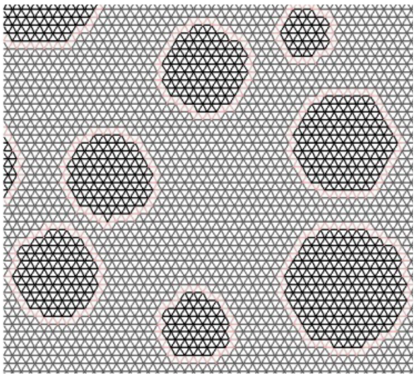

Figure 2. A lattice mesh with various elements; the dark elements are aggregate, the gray ones are matrix, and the light elements are interface beams.

2.1. The stiffness matrix of lattice element

In lattice model, the beam element has three degrees of freedom at each node, including the normal displacement, shear displacement and bending moment, as shown in Figure 3. By superposing a beam element of four DOFs with a simple rod element of two DOFs, the stiffness matrix of a general beam element in lattice model can be defined as:

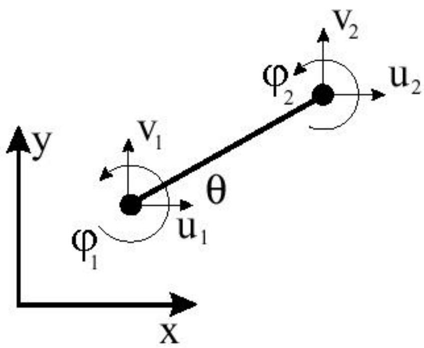

Figure 3. The degrees of freedom for a 2D beam element.

$$\mathbf{K}_{\text{beam}} = \begin{bmatrix} B_{11} & B_{12} & -B_{11} & B_{12} \\ & B_{22} & -B_{12} & B_{24} \\ & & B_{11} & -B_{12} \\ sym & & & B_{22} \end{bmatrix} \quad \text{and} \quad \mathbf{K}_{\text{rod}} = \frac{AE}{l}\begin{bmatrix} 1 & -1 \\ -1 & 1 \end{bmatrix} \tag{7}$$

$$\mathbf{K}_{\text{rod+beam}} = \begin{bmatrix} AE/l & 0 & 0 & -AE/l & 0 & 0 \\ & B_{11} & B_{12} & 0 & -B_{11} & B_{12} \\ & & B_{22} & 0 & -B_{12} & B_{24} \\ & & & AE/l & 0 & 0 \\ & sym & & & B_{11} & -B_{12} \\ & & & & & B_{22} \end{bmatrix} \tag{8}$$

where the vector of nodal degrees-of-freedom is defined as $\mathbf{u} = \{u_1 \ v_1 \ \varphi_1 \ u_2 \ v_2 \ \varphi_2\}^T$, and the vector of external forces as $\mathbf{f} = \{N_1 \ V_1 \ M_1 \ N_2 \ V_2 \ M_2\}^T$. In above relation, B_{ij} is defined based on the theory of Timoshenko beam as:

$$B_{11} = \frac{G\hat{A}}{l} \qquad B_{12} = \frac{G\hat{A}}{2} \qquad B_{22} = \frac{G\hat{A}l}{4} + \frac{E^b I}{l} \qquad B_{24} = \frac{G\hat{A}l}{4} - \frac{E^b I}{l} \tag{9}$$

where $G = E^b/[2(1+\upsilon^b)]$, and GA denotes the shear rigidity. $\hat{A} = A/\alpha$, with α denoting a correction factor, which is defined for the cross-sectional warping as [15]:

$$\alpha = \begin{cases} \dfrac{12 + 11\upsilon^b}{10 + 10\upsilon^b} & \text{for rectangular cross sections} \\ \dfrac{7 + 6\upsilon^b}{6 + 6\upsilon^b} & \text{for circular cross sections} \end{cases} \tag{10}$$

In case of the Euler–Bernoulli theory, the values of B_{ij} are defined as:

$$B_{11} = \frac{12EI}{l^3} \qquad B_{12} = \frac{6EI}{l^2} \qquad B_{22} = \frac{4EI}{l} \qquad B_{24} = \frac{2EI}{l} \tag{11}$$

In order to derive the total stiffness matrix, we need to obtain the global stiffness matrix by assembling the stiffness matrix of each beam element in a standard manner using the Jacobean matrix. However in the standard lattice model, each element regardless of its phase is assigned to the horizontal direction with $\theta = 0$, inclined with $\theta = 60^{\circ}$, or inclined with $\theta = 120^{\circ}$. Thus, the stiffness matrix does not need any modification for assembling in the global matrix, and can be obtained using the rotation matrix as:

$$\widehat{\mathbf{K}} = \mathbf{\Gamma}^T \mathbf{K}_{\text{rod+beam}} \mathbf{\Gamma} \tag{12}$$

where:

$$\mathbf{\Gamma} = \begin{bmatrix} \cos\theta & \sin\theta & 0 & 0 & 0 & 0 \\ -\sin\theta & \cos\theta & 0 & 0 & 0 & 0 \\ 0 & 0 & 1 & 0 & 0 & 0 \\ 0 & 0 & 0 & \cos\theta & \sin\theta & 0 \\ 0 & 0 & 0 & -\sin\theta & \cos\theta & 0 \\ 0 & 0 & 0 & 0 & 0 & 1 \end{bmatrix} \tag{13}$$

2.2. The fracture criteria

In fracture mechanics, it has been shown that the meso-, or micro-scale simulation can be used by employing the simple constitutive laws. It implies that although fracture is a nonlinear, inelastic phenomenon in macro-scale modeling of concrete, we can use the linear elastic beam elements in the meso- or micro-scale simulation. Most of research works in lattice modeling of fracture in concrete have been used by a simple stress or strain criterion, as the fracture criteria. It means that whenever an element reaches the specific criterion, that element can be removed from the lattice mesh. It is noteworthy to be explained that the removal of an element will not cause any numerical instability and would be the best way of simulation for the fracture analysis of concrete. In this study, an axial strain criterion proposed by Karihaloo et al. [14] is used as:

$$\varepsilon_{\text{failure}} = \frac{[(u_2 - u_1)\cos\theta + (v_2 - v_1)\sin\theta + |\varphi_1 - \varphi_2|\, h\gamma/2]}{l} \tag{14}$$

in which each element that its strain exceeds the above limit will be removed from the model. In relation (14), u_i , v_i and φ_i are the degrees of freedom, as shown in Figure 3, γ is a coefficient that determines the contribution of the curvature in strain calculations, considered as $\gamma = 0.005$, and h denotes the depth of the beam element.

3. Dynamic lattice model

The dynamic lattice model can be formulated based on the standard continuum medium concept of dynamic behavior. In dynamic continuum medium, each node of lattice beam element includes two additional components, i.e. the velocity and acceleration, in which these two components are incorporated into the damping and mass matrices. It is assumed that the mass of each element concentrates on its ends, and as a result the mass matrix is diagonal with the components defined as [8]:

$$\mathcal{M} = \frac{\sqrt{3}\rho l^2 t_b}{2} \quad , \quad \mathcal{J} = \frac{5\rho l^4 t_b}{8}\left(\frac{\sqrt{3}}{9} - \frac{3\pi}{64}\right) \tag{15}$$

where $\mathcal{M}$ is the diagonal component of the first two DOFs, $\mathcal{J}$ is the diagonal component of the third DOF at each node, and ρ denotes the density. The damping matrix is assumed to be a linear combination of the mass matrix M and the stiffness matrix , i.e. $C = \bar{\alpha}M + \bar{\beta}K$, in which parameters $\bar{\alpha}$ and $\bar{\beta}$ are chosen as $\bar{\alpha} = 0.5$ and $\bar{\beta} = 0.001$ for concrete [8].

In order to perform the numerical modeling of dynamic analysis, the Newmark technique is applied here. In this method, the accuracy and convergency are satisfied by using two parameters, called γ_1 and γ_2, through the following relations:

$$\dot{u}_{i+1} = \dot{u}_i + [(1-\gamma_1)\Delta t]\ddot{u}_i + (\gamma_1 \Delta t)\ddot{u}_{i+1} \tag{16}$$

$$u_{i+1} = u_i + (\Delta t)\dot{u}_i + [(0.5-\gamma_2)(\Delta t)^2]\ddot{u}_i + [\gamma_2(\Delta t)^2]\ddot{u}_{i+1} \tag{17}$$

The technique is unconditionally stable, if $\Delta t/T_n \le 1/\pi\sqrt{2(\gamma_1 - 2\gamma_2)}$, $\gamma_1 \le 1/2$ and $\gamma_2 \le 1/4$ [16]. If $\gamma_1 = 1/2$ and $\gamma_2 = 1/4$, the Newmark method is called as the *average acceleration method*, since the acceleration in an interval time-step is assumed to be constant, i.e.

$$\begin{aligned} \dot{u}_{i+1} &= \dot{u}_i + \frac{1}{2}\Delta t\, \ddot{u}_i + \frac{1}{2}\Delta t\, \ddot{u}_{i+1} \\ u_{i+1} &= u_i + \Delta t\, \dot{u}_i + \frac{1}{4}\Delta t^2\, \ddot{u}_{i+1} \end{aligned} \tag{18}$$

or:

$$\begin{aligned} \Delta\dot{u}_i &= \frac{2}{\Delta t}\Delta u_i - 2\dot{u}_i \\ \Delta\ddot{u}_i &= \frac{4}{\Delta t^2}(\Delta u_i - \Delta t\, \Delta\dot{u}_i) - 2\ddot{u}_i \end{aligned} \tag{19}$$

If $\gamma_1 = 1/2$ and $\gamma_2 = 1/6$, the Newmark method is called as the *linear acceleration method*. In this case, the convergency condition is given by $\Delta t/T_n \leq \sqrt{3}/\pi$ and in an interval time-step, we have:

$$\dot{u}_{i+1} = \dot{u}_i + \frac{1}{2}\Delta t\, \ddot{u}_i + \frac{1}{2}\Delta t\, \ddot{u}_{i+1}$$
$$u_{i+1} = u_i + \Delta t\, \dot{u}_i + \frac{1}{3}\Delta t^2\, \ddot{u}_i + \frac{1}{6}\Delta t^2\, \ddot{u}_{i+1} \tag{20}$$

or:

$$\Delta\dot{u}_i = \frac{3}{\Delta t}\Delta u_i - 3\dot{u}_i - \frac{1}{2}\Delta t\, \ddot{u}_i$$
$$\Delta\ddot{u}_i = \frac{6}{\Delta t^2}(\Delta u_i - \Delta t\, \Delta\dot{u}_i) - 3\ddot{u}_i \tag{21}$$

In lattice beam model, the natural period of one single beam element T_n would be extremely small, since the lattice beam element has very small length (0.5 to 2 mm). Thus, Δt must be unfeasibly small to satisfy the convergency condition. As a result, the unconditionally convergence method of average acceleration method is preferred here for dynamic modeling of crack propagation. The equilibrium equation of dynamic continuum medium can be written as:

$$M\ddot{u}_i + C(t)\dot{u}_i + \widehat{K}(t)u_i = P(t) \tag{22}$$

or in an incremental form:

$$M\Delta\ddot{u}_i + C(t)\Delta\dot{u}_i + \Delta C\dot{u}_i + K(t)\Delta u_i + \Delta K u_i = \Delta P \tag{23}$$

where M is the mass matrix, which is diagonal and constant, $\widehat{K}$ is the stiffness matrix defined in (12) and C is the damping matrix. Applying the average acceleration method and using the derived relations for $\Delta\dot{u}_i$ and $\Delta\ddot{u}_i$, equation (23) can be rewritten as:

$$\mathbb{K}\,\Delta u_i = \Delta\mathbb{P} \tag{24}$$

where:

$$\mathbb{K} = \widehat{K}(t) + \frac{2}{\Delta t}C(t) + \frac{4}{\Delta t^2}M \tag{25}$$

$$\Delta\mathbb{P} = \Delta P + \left(\frac{4}{\Delta t}M + 2C\right)\dot{u}_i + 2M\ddot{u}_i - \Delta C\dot{u}_i - \Delta\widehat{K}u_i \tag{26}$$

Based on equation (24), Δu_i can be calculated by a simple linear equation at each time step, and the values of u_{i+1} and $\dot{u}_{i+1}$ can be then obtained from relations (19), however for a better acccuracy, it is preferred to evaluate $\ddot{u}_{i+1}$ through the equilibrium equation (22), i.e.

$$M\ddot{u}_{i+1} = P(t) - C(t)\dot{u}_{i+1} - \widehat{K}(t)u_{i+1} \tag{27}$$

It must be noted that the unconditional convergency can be obtained at the cost of losing accuracy. For this reason, the numerical simulation has to be in a limited range of loading rate, since the high loading rate causes some fluctuations in the snap-back part of force-displacement curve, which is the result of numerical instability. One possible solution for this phenomenon is to implement the dominant mode shapes of the model, which has a widespread application in the dynamic analysis of tall structures [16].

4. Numerical simulation results

In order to demonstrate the performance of proposed dynamic lattice model, several practical examples are analyzed numerically. A computer code was developed based on the computational algorithm presented in preceding sections to perform the numerical simulations using the parallel processing. A compressed sparse row format is used to store the global stiffness matrix, and a math kernel library sparse solver is engaged that uses the CGS method with the privilege of parallelism. Based on the sparse format and the parallel CGS solver, the computer code is fast enough to simulate large numerical examples that have never been experienced before. In order to simulate and predict the failure of system, according to the displacement increment at each time step, if the strain of lattice element reaches the strength criterion, the element is removed from the system, and the stiffness matrix and load vector are updated to restart the simulation from the previous displacement increment.

The first example is the well-known simple tension experiment, which illustrates the perfect pattern of mode I crack propagation [12,14,17]. The second example is the Nooru-Mohamed [18] mixed-mode fracture experiment chosen to demonstrate the capability of proposed model in complex boundary conditions. For each numerical simulation, the aggregate formation is preserved constant and the effects of model parameters are investigated. Both experiments are performed in three different phases, including the static model, the dynamic model with load rate of $0.001\ \mathrm{cm/s}$, and the dynamic model with load rate of $0.1\ \mathrm{cm/s}$. Also, the dimensionless ratio of bending to shear stiffness of element β is chosen as 0.946, and the thickness of beam element $t^b = 0.738$, however they do not have any significant effects on numerical results.

4.1. The simple tension experiment

The first example is chosen to demonstrate the performance of proposed lattice model for a simple tension experiment performed by Prado and van Mier [17], as shown in Figure 4. Due to the fact that there is no notch or initial crack in this example, the micro cracks and inhomogeneity of the specimen are the main components of fracture in the material. On the other hand, models that consider concrete as a homogeneous material are incapable of handling this phenomenon [19]. In order to perform the lattice analysis, a sample of 100x100 mm with 11658 nodes and 34542 elements is modeled using lattice beam elements, as shown in Figure 5. The specimen is fixed at the bottom edge and is subjected to prescribed displacement at the top edge. The sample undergoes the displacement control of $0.1\ \mu$m loading step for quasi-static analysis, and $0.001\ \mathrm{cm/s}$ and $0.1\ \mathrm{cm/s}$ for dynamic modeling until $15.0\ \mu$m. The time steps are assumed to be $\Delta t = 0.001$ s and $\Delta t = 0.00001$ s , which is equivalent to the total simulation of 1.5 s and 0.015 s, respectively. The aggregate distribution is in accordance with Table 1, which is common among various researchers. Also, the assigned material characteristics in continuum medium are given in Table 2. Aggregates are randomly generated and have the mentioned minimum distances. The ‘interface’ elements include the weakest material properties, and the micro cracks are expected to initiate from these elements. The distribution of the formation of aggregates, including the ‘aggregate’, ‘matrix’ and ‘interface’ lattice beams, is shown in Figure 5.

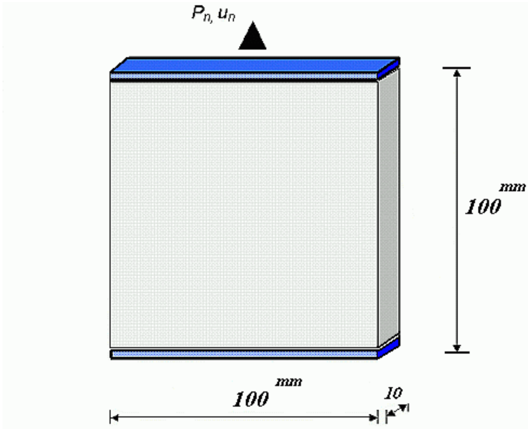

Figure 4. The simple tension test; Problem definition.

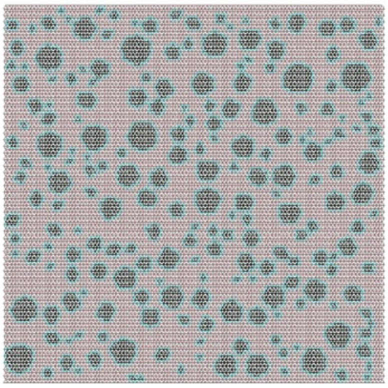

Figure 5. The lattice model of simple tension experiment.

Table 1. Particle Distribution.

Diameter (mm)	Number
80	5
70	10
60	20
50	30
40	40
30	50
20	60

Table 2. The elastic properties of continuum medium.

Phase	Elasticity (N/cm^2)	Poisson ratio	Tensile strength (N/cm^2)
matrix	3125500	0.261	500
aggregate	8751400	0.261	1000
interface	3125500	0.261	150

In all simulations, the specimen deforms in a linear, elastic manner until the micro-cracks initiate around aggregates. In this case, the stiffness of those lattice elements that reach the strength criterion is eliminated from the global stiffness matrix. In Figure 6, the force-displacement curves are plotted for static and dynamic analyses. The predicted crack trajectory of simple tension test is shown in Figure 7 for static and dynamic simulations. As can be seen there are no considerable differences between the crack patterns of two analyses. In all simulations, the main crack appears at the mid-left of specimen and propagates along the horizontal direction, as expected. The predicted crack patterns are in complete agreement with that reported by Prado and van Mier [17] in Figure 8. It must be noted that there are some ramifications around the main crack, which can be clearly observed in the fracture of concrete, however – cannot be simulated with other numerical techniques, such as the adaptive FEM, or X-FEM approaches.

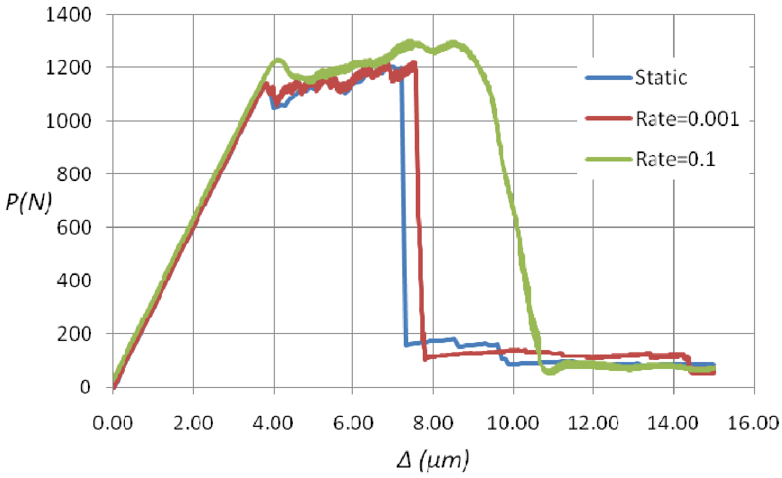

Figure 6. The force-displacement curves for static and dynamic simulations.

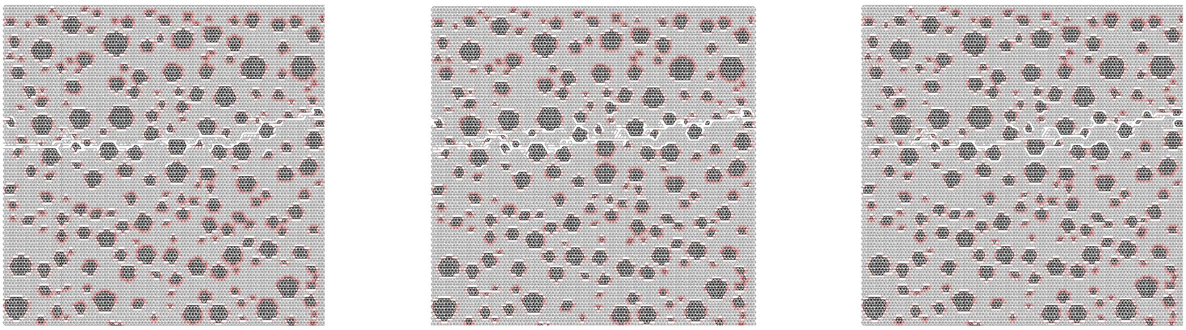

(a) (b) (c)

Figure 7. The crack trajectory of simple tension experiment; (a) the static model, (b) the dynamic model with load rate of 0.001 cm/s, (c) the dynamic model with load rate of 0.1 cm/s.

Figure 8. The predicted crack trajectory for simple tension test reported by Prado and van Mier [17].

In Figure 9, the distributions of normal stress contours are shown for the static analysis of simple tension test at various stages of crack formation, including: the micro-crack formation, main crack initiation, and complete failure. In Figure 10, a comparison of the force-displacement curves is performed between the static analysis and dynamic simulation with load rate of $0.001\ \mathrm{cm/s}$. Due to low load rate of dynamic analysis, the results of dynamic simulation are similar to those obtained from the static analysis. It can also be seen from the distribution of normal stress contours shown in Figure 11 at various stages of loading. In order to present the performance of dynamic simulation, the analysis is carried out once again with load rate of $0.1\ \mathrm{cm/s}$. The difference between the force-displacement curve of static and dynamic analyses are obvious in Figure 12. It must be noted that the initiation of micro cracks in static analysis occurs at the displacement of $3.6\ \mu\mathrm{m}$ and load of $1080\ \mathrm{N}$, while in dynamic analysis with load rate of $0.1\ \mathrm{cm/s}$, it happens at the displacement of $4.1\ \mu\mathrm{m}$ and load of $1210\ \mathrm{N}$. Also presented in Figure 13 is the distribution of normal stress contours at various stages of crack formation for load rate of $0.1\ \mathrm{cm/s}$.

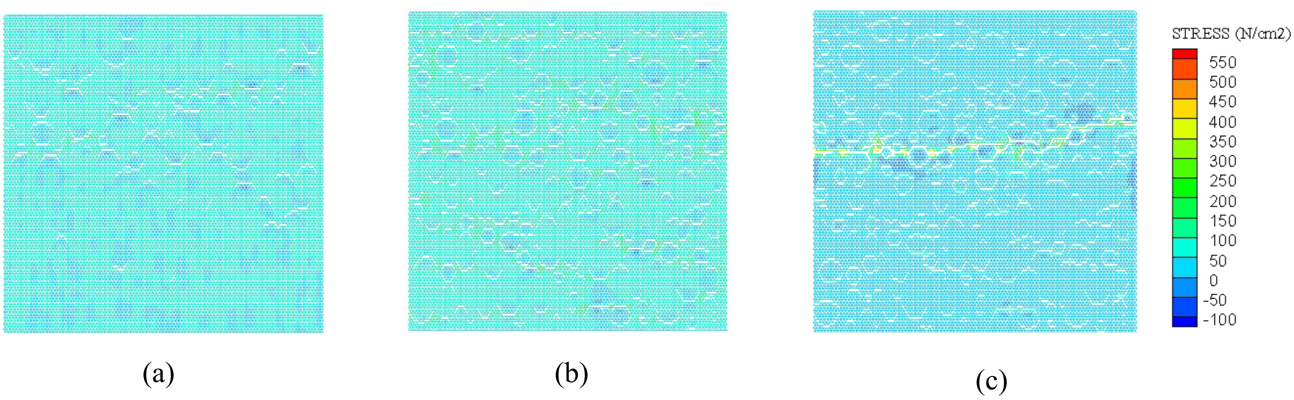

Figure 9. The distribution of normal stress contours for the static analysis of simple tension test; (a) the micro-crack formation, (b) the main crack initiation, (c) the complete failure.

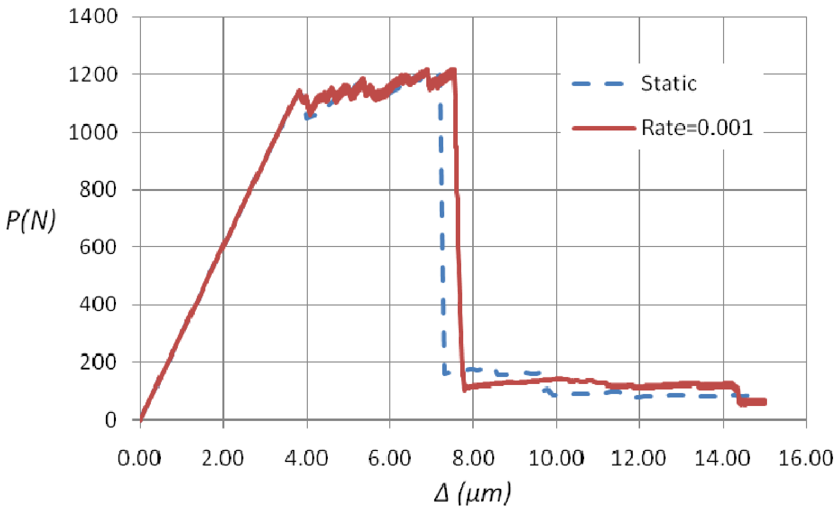

Figure 10. A comparison of the force-displacement curve between the static analysis and dynamic modeling with load rate of 0.001 cm/s.

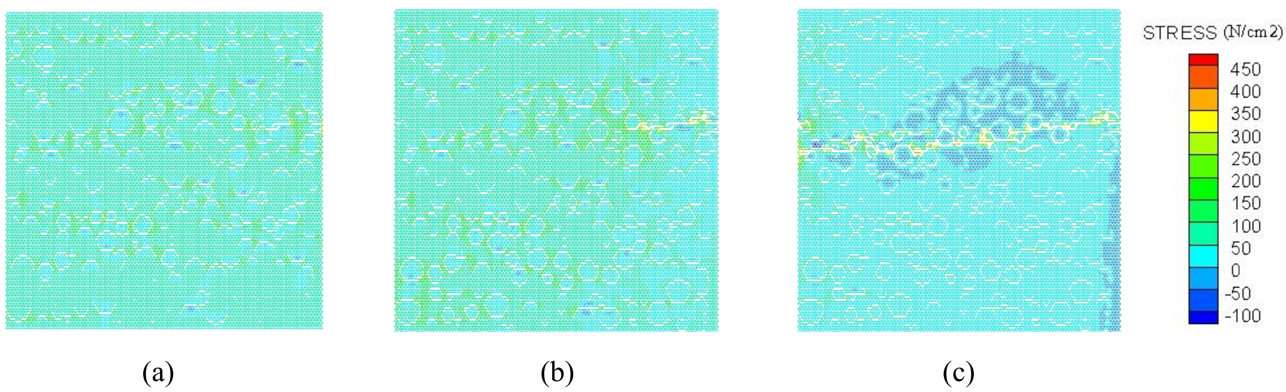

Figure 11. The distribution of normal stress contours for dynamic analysis of simple tension test with load rate of 0.001 cm/s; (a) the micro-crack formation, (b) the main crack initiation, (c) the complete failure.

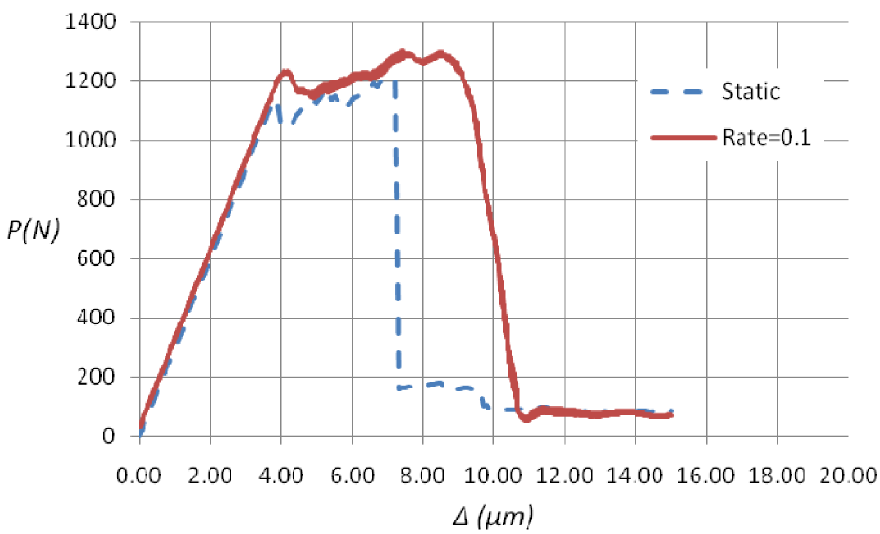

Figure 12. A comparison of the force-displacement curve between the static analysis and dynamic modeling with load rate of 0.1 cm/s.

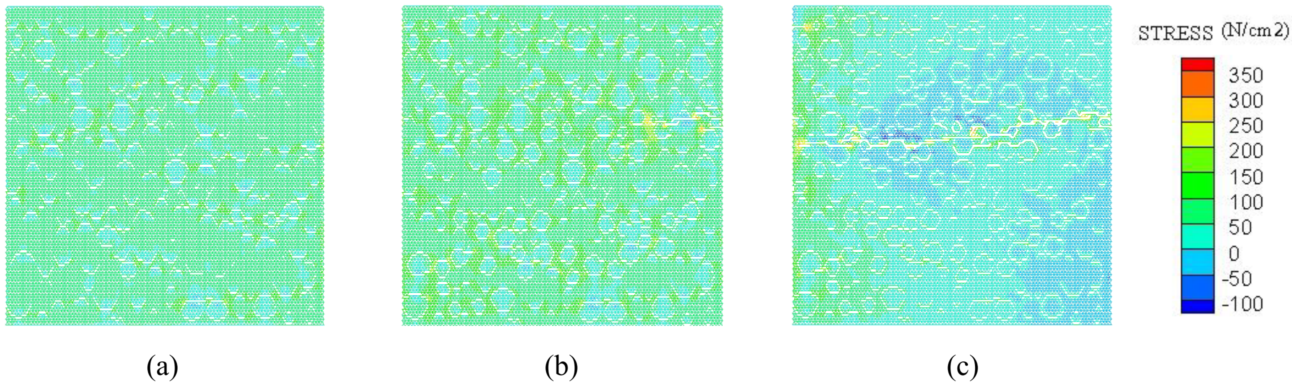

Figure 13. The distribution of normal stress contours for dynamic analysis of simple tension test with load rate of 0.1 cm/s; (a) the micro-crack formation, (b) the main crack initiation, (c) the complete failure.

4.2. The Nooru-Mohamed experiment

The next example is chosen to illustrate the capability of proposed lattice technique in modeling of mixed-mode fracture experiment, originally performed by Nooru-Mohamed [18]. This example was also modeled by Moslemi and Khoei [20] to demonstrate their 3D adaptive finite element modeling in numerical simulation of crack propagation. A concrete specimen of 100x100x50 mm with two notches, as shown in Figure 14, is subjected to different proportional and non proportional load paths. The test applies tensile and shear loads to a double-edge-notched specimen (DENS) simultaneously, which causes the mixed-mode fracture phenomenon and illustrates tracking crack paths with respect to two non-interacting cracks. In order to compare the results of proposed computational algorithm with those experimentally reported by Nooru-Mohamed [18], two load paths proposed in reference [18], i.e. the load paths of (6a) and (6b), are employed here. These two proportional paths are modeled using a displacement control manner with $\delta_t/\delta_s = 1$ and $\delta_t/\delta_s = 2$, respectively, with δ_t denoting the tensile prescribed displacement and δ_s the shear prescribed displacement. The geometry and boundary conditions of the double-edge-notched specimen are shown in Figure 14. The distribution of ‘aggregate’, ‘matrix’ and ‘interface’ lattice beams are depicted in Figure 15. The maximum size of aggregate for this specimen is $d_{\max} = 2$ mm with 500 aggregates, as shown in this figure. The material properties of specimen are similar to previous example, as given in Table 2. In order to investigate the effects of dynamic simulation, similar pattern of aggregate distribution is used for all numerical simulations. Also, to compare the results of static and dynamic simulations, the dynamic analysis is carried out using two load rates of $0.001\ \mathrm{cm/s}$ and $0.1\ \mathrm{cm/s}$.

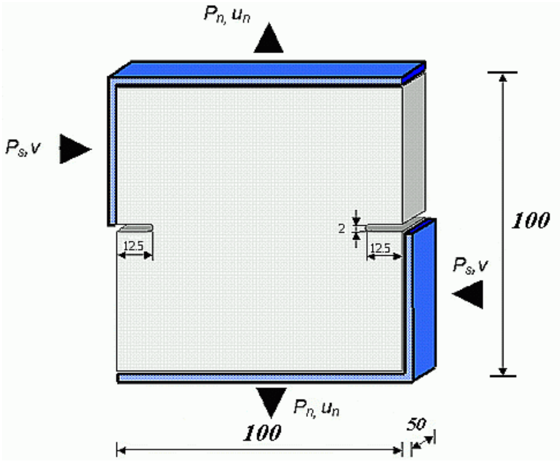

Figure 14. The Nooru-Mohamed shear test; Problem definition.

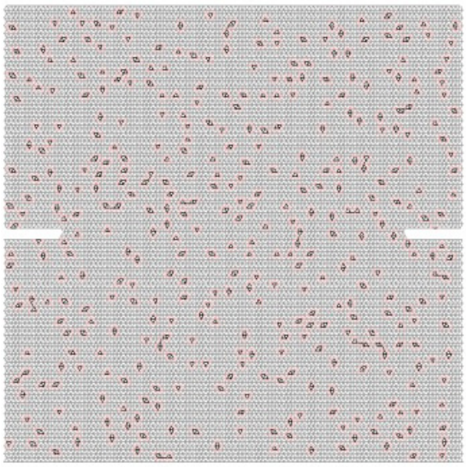

Figure 15. The lattice model of Nooru-mohamed test.

In Figure 16, the predicted crack trajectory obtained by experiment is shown for load path (6a). The distributions of normal stress contour together with the crack trajectory are presented for load path (6a) in Figure 17 for static and dynamic simulations. The crack trajectory of specimen is in good agreement with that reported in Figure 16 experimentally. In Figure 18, the variations of normal-force with displacement are plotted for static and dynamic simulations. A noticeable difference can be observed between experimental and numerical results, since a 2D numerical modeling is adopted here. The variations of shear-force with displacement are plotted in Figure 19 for static and dynamic analyses. A good agreement can be seen between experimental and numerical results. As can be observed from Figures 18 and 19, the results of dynamic simulations are very close to those obtained by the static analysis, since the rate of normal to shear displacements is chose as $\delta_t/\delta_s = 1$ for load path (6a).

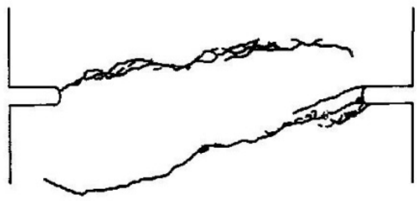

Figure 16. The predicted crack trajectory for load path (6a) obtained by experiment.

In order to demonstrate the performance of dynamic simulation, the analysis is carried out for the load path (6b) with the rate of normal to shear displacements $\delta_t/\delta_s = 2$. In Figure 20, the distribution of normal stress contours are presented together with the crack trajectory for load path (6b) in static and dynamic simulations with load rates of 0.001 cm/s and 0.1 cm/s. The variations of normal-force with displacement are plotted in Figure 21 for experimental and numerical results. Also plotted in Figure 22 are the variations of shear-force with displacement for different simulations. Finally, in order to illustrate the dynamic effect of load path (6b), the variation of normal-force with displacement corresponding to dynamic simulation with load rate of 0.2 cm/s is added in Figure 23. Clearly, it can be observed from this figure that the increasing of dynamic load rate causes the convergency between the dynamic analysis and experimental results.

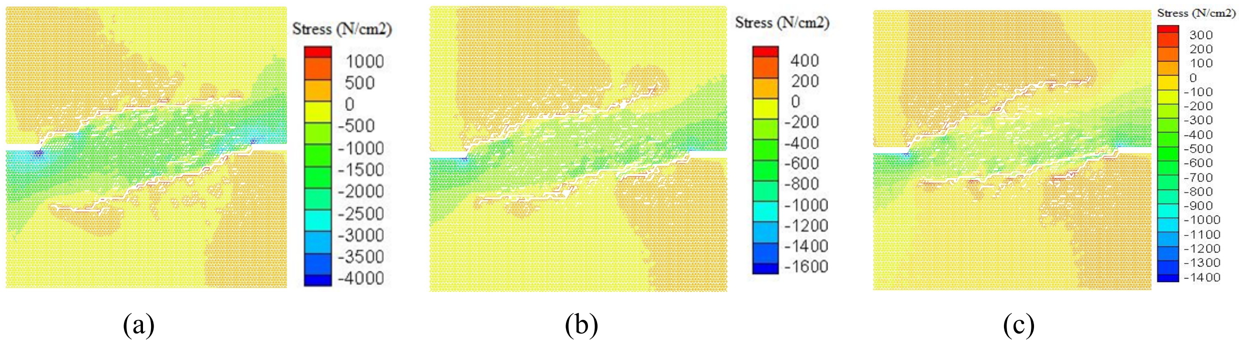

Figure 17. The normal stress contours together with the crack trajectory for load path (6a) of the Nooru-mohamed test; (a) the static model, (b) the dynamic model with load rate of 0.001 cm/s, (c) the dynamic model with load rate of 0.1 cm/s.

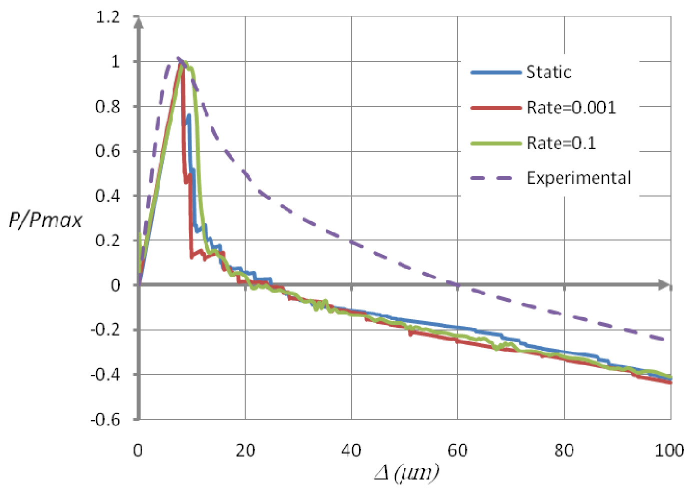

Figure 18. The normal-force vs. displacement curves for static and dynamic simulations of load path (6a).

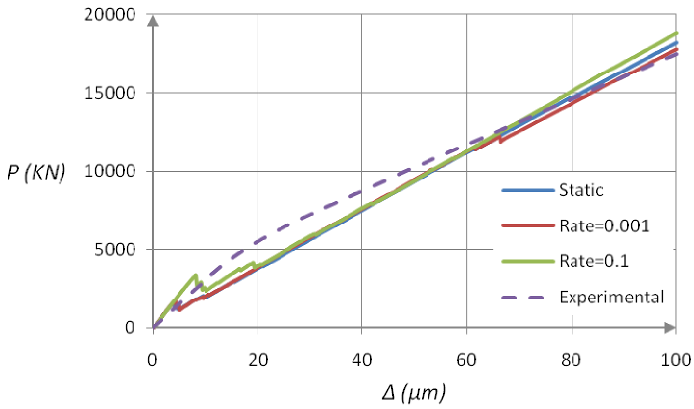

Figure 19. The shear-force vs. displacement curves for static and dynamic simulations of load path (6a).

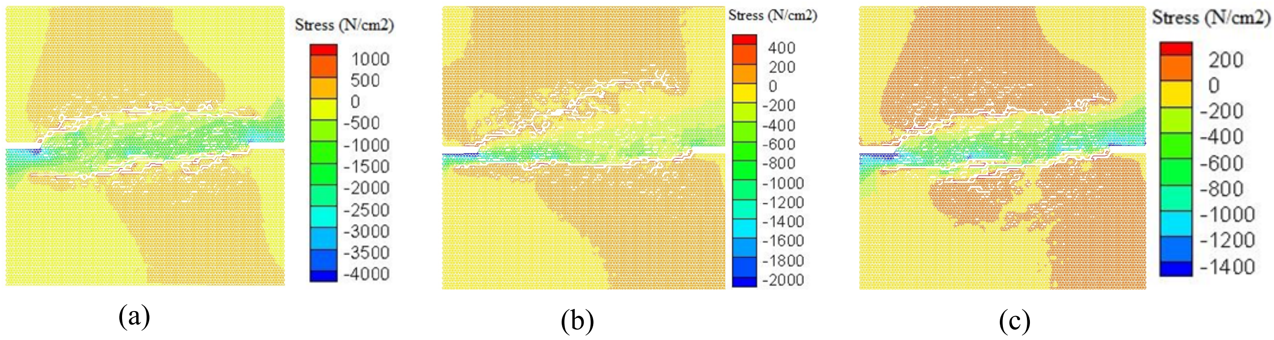

Figure 20. The normal stress contours together with the crack trajectory for load path (6b) of the Nooru-mohamed test; (a) the static model, (b) the dynamic model with load rate of 0.001 cm/s, (c) the dynamic model with load rate of 0.1 cm/s.

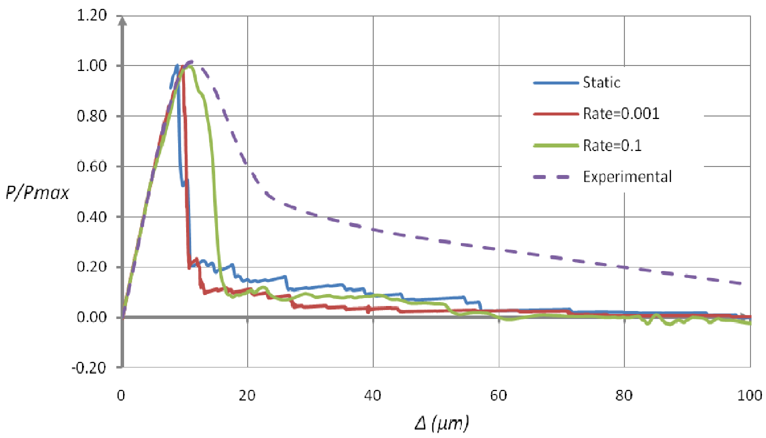

Figure 21. The normal-force vs. displacement curves for static and dynamic simulations of load path (6b).

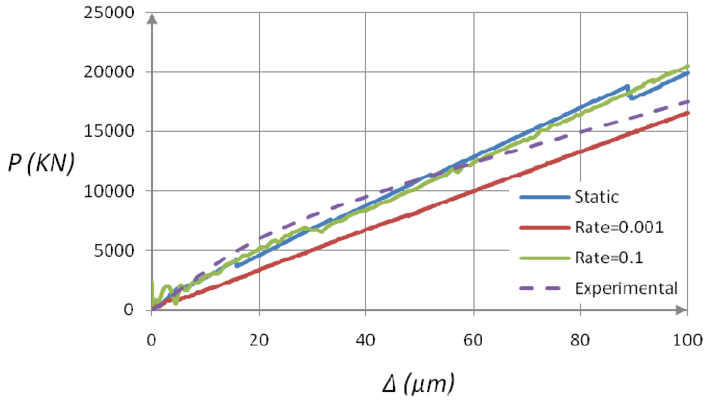

Figure 22. The shear-force vs. displacement curves for static and dynamic simulations of load path (6b).

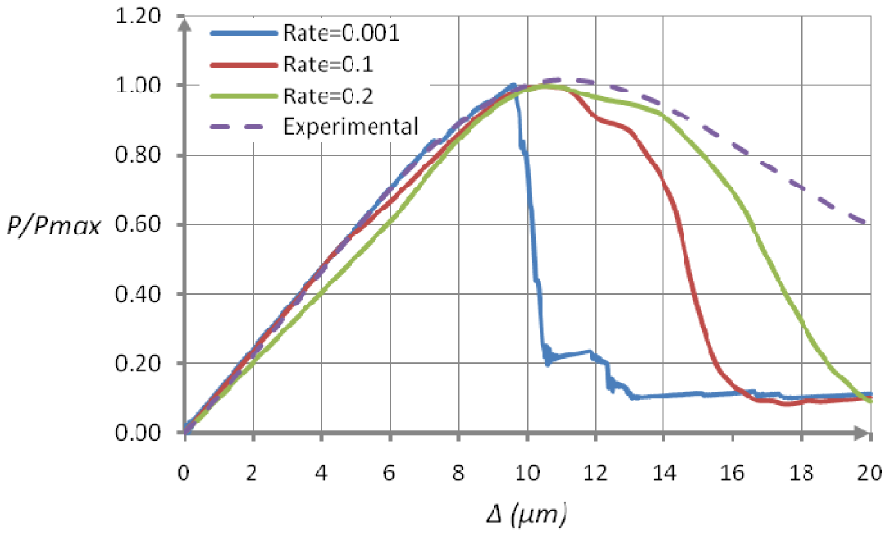

Figure 23. The normal-force vs. displacement curves for static and dynamic simulations with various load rates for load path (6b).

5. Conclusion

In the present paper, a meso-scale model based on the lattice beam element technique was developed to investigate the mechanical behavior of three-phase inhomogeneous materials in static and dynamic cases. The Timoshenko beam theory was applied for lattice beam elements, in which three degrees-of-freedom were assumed at each node of lattice element, including the normal displacement, shear displacement and bending moment. The mechanical properties of lattice element connection were derived using the non-local continuum theory. The dynamic analysis was carried out based on the average acceleration method in the Newmark approach. The distribution of aggregates in lattice model was generated based on the location of aggregates on lattice mesh in a decelerating manner. An axial strain criterion was proposed to model the fracture of material, in which each element that its strain exceeds the strength criterion was removed from the model. A computer program was developed based on the proposed computational algorithm with the capability of sparse format and parallel CGS solver to perform the numerical simulations using the parallel processing.

Finally, two experimental tests, including the simple tension test and the Nooru-Mohamed test, were modeled to illustrate the capability of lattice beam model in simulation of crack propagation in concrete. Both experiments were performed in three different phases, including the static model, the dynamic model with load rate of $0.001\ \mathrm{cm/s}$, and dynamic model with load rate of $0.1\ \mathrm{cm/s}$. The distribution of normal stress contours were presented as well as the crack trajectory for static and dynamic simulations. The variations of normal and shear forces were plotted with displacement for all simulations. The first example was a simple tension experiment chosen to illustrates the pattern of mode I crack propagation. The example clearly shown the applicability of lattice model for a specimen with no notch or initial crack, As a result, the micro cracks and inhomogeneity of the specimen were the main components of fracture in the concrete. The next example was the Nooru-Mohamed experiment chosen to illustrate the capability of proposed model in simulation of mixed-mode fracture. The test was simulated by applying the tensile and shear loads to a double-edge-notched specimen simultaneously, for two proportional load paths, i.e. $\delta_t/\delta_s = 1$ and $\delta_t/\delta_s = 2$. It was shown that for load path (6a) with $\delta_t/\delta_s = 1$, the results of dynamic simulations are very close to those obtained by the static analysis. However, the effects of dynamic simulation can be clearly observed for load path (6b) corresponding to the rate of normal to shear displacements $\delta_t/\delta_s = 2$. It was also shown that the crack trajectory of specimen is in good agreement with that reported experimentally.

References

[1] A. Hrennikoff, Solution of problems of elasticity by the framework method, *J. Appl. Mech.,* 12 (1941) 169–175.

[2] J. Kozicki, J. Tejchman, Effect of aggregate structure on fracture process in concrete using 2D lattice model, *Arch. Mech.*, 59 (2007) 365–384.

[3] J.X. Liu, S.C. Deng, J. Zhang, N.G. Liang, Lattice type of fracture model for concrete, *Theo. Appl. Fract. Mech.*, 48 (2007) 269–284.

[4] H.J. Herrmann, A. Hansen, S. Roux, Fracture of disordered, elastic lattices in two dimensions, *Phys. Rev.*, 39 (1989) 637–648.

[5] H. Kim, W.G. Buttlar, Discrete fracture modeling of asphalt concrete, *Int. J. Solids Struct.,* 46 (2009) 2593–2604.

[6] A. Spagnoli, A micromechanical lattice model to describe the fracture behavior of engineered cementitious composites, *Comput. Mater. Sci.*, 46 (2009) 7–14.

[7] J.X. Liu, Z.Y. Zhao, S.C. Deng, N.G. Liang, Modified generalized beam lattice model associated with fracture of reinforced fiber/particle composites, *Theo. Appl. Fract. Mech.*, 50 (2008) 132–141.

[8] J.X. Liu, S.C. Deng, N.G. Liang, Comparison of the quasi-static method and the dynamic method for simulating fracture processes in concrete, *Comput. Mech.*, 41 (2008) 647–660.

[9] G. Lilliu, J.G.M. van Mier, 3D lattice type fracture model for concrete, *Eng. Fract. Mech., 70 (*2003) 927–941.

[10] E. Schlangen, E.J. Garboczi, New method for simulating fracture using an elastically uniform random geometry lattice, *Int. J. Eng. Science.*, 34 (1996) 1131–1144.

[11] G. Cusatis, Z.P. Bazant, L. Cedolin, Confinement-shear lattice model for concrete damage in tension and compression, I. Theory, *J. Eng. Mech.,* 129 (2003) 1439–1448.

[12] G. Cusatis, Z.P. Bazant, L. Cedolin, Confinement-shear lattice CSL model for fracture propagation in concrete, *Comp. Meth. Appl. Mech. Eng.,* 195 (2006) 7154–7171.

[13] J. Kozicki, J. Tejchman, Modeling of fracture process in concrete using a novel lattice model, *Granular Matter.*, 10 (2008) 377-388.

[14] B.L. Karihaloo, P.F. Shao, Q.Z. Xiao, Lattice modelling of the failure of particle composites, *Eng. Fract. Mech.*, 70 (2003) 2385–2406.

[15] G.R. Cowper, The shear coefficient in Timoshenko's beam theory, *J. Appl. Mech.*, 33 (1966) 335–340.

[16] R.W. Clough, J. Penzien, *Dynamics of Structures*, McGraw-Hill, New York, 1993.

[17] E.P. Prado, J.G.M. van Mier, Effect of particle structure on mode I fracture process in concrete, *Eng. Fract. Mech.*, 70 (2003) 1793–1807.

[18] M.B. Nooru-Mohamed, Mixed-mode fracture of concrete: An experimental approach, *PhD thesis*, Delft University of Technology, The Netherlands, 1992.

[19] A.R. Khoei, H. Azadi, H. Moslemi, Modeling of crack propagation via an automatic adaptive mesh refinement based on modified superconvergent patch recovery technique, *Eng. Fract. Mech.,* 75 (2008) 2921–2945.

[20] H. Moslemi, A.R. Khoei, 3D adaptive FE modeling of non-planar curved crack growth using the weighted super-convergent patch recovery method, *Eng. Fract. Mech.,* 76 (2009) 1703–1728.